Forcing for statistically stationary compressible isotropic turbulence

Mark R. Petersen[a)] and Daniel Livescu[b)]

Los Alamos National Laboratory, Los Alamos, New Mexico 87544, USA

Linear forcing has been proposed as a useful method for forced isotropic turbulence simulations because it is a physically realistic forcing method with a straightforward implementation in physical-space numerical codes [T. S. Lundgren, "Linearly forced isotropic turbulence," *Annual Research Briefs* (Center for Turbulence Research, Stanford, CA, 2003), p. 461; C. Rosales and C. Meneveau, "Linear forcing in numerical simulations of isotropic turbulence: Physical space implementations and convergence properties," Phys. Fluids **17**, 095106 (2005)]. Here, extensions to the compressible case are discussed. It is shown that, unlike the incompressible case, separate solenoidal and dilatational parts for the forcing term are necessary for controlling the stationary state of the compressible case. In addition, the forcing coefficients can be cast in a form that allows the control of the stationary state values of the total dissipation (and thus the Kolmogorov microscale) and the ratio of dilatational to solenoidal dissipation. Linear full spectrum forcing is also compared to its low wavenumber restriction. Low wavenumber forcing achieves much larger Taylor Reynolds number at the same resolution. Thus, high Reynolds number asymptotics can be more readily probed with low wavenumber forced simulations. Since, in both cases, a solenoidal/dilatational decomposition of the velocity field is required, the simplicity of the full spectrum linear forcing implementation in physical-space numerical codes is lost. Nevertheless, low wavenumber forcing can be implemented without using a full Fourier transform, and so is computationally less demanding. © *2010 American Institute of Physics*. [doi:10.1063/1.3488793]

I. INTRODUCTION

Numerical simulations to investigate the behavior of isotropic turbulence still play an important role in turbulence research, especially since the advances in supercomputing power now allow simulations at Reynolds numbers comparable or even larger than those obtained in laboratory experiments.[1] If a forcing term is added to the equations, then the flow could reach a statistically stationary state, where the injection rate (usually at large scales) is equal to the rate of energy dissipated at small scales. Forcing has several advantages. The Reynolds number of the simulation can be increased considerably; statistics can be averaged over time, which decreases the statistical variability due to transient effects; and natural systems are usually forced.

Forcing in nature is due to large-scale effects, for example, solar induced, buoyancy-driven convection in the atmosphere. The characteristics of turbulence at much smaller scales are thought to be independent of the nature of the forcing, which is why turbulence is often studied in an idealized, triply periodic domain. There are several ways in which the forcing can be applied. To minimize the long range correlations by providing an explicit randomization mechanism, the forcing coefficients can be calculated from a random process.[2,3] However, in this case, the external randomness may affect the intrinsic randomness associated with the turbulence dynamics.[1,4] To avoid this concern, the forcing in this work is chosen to be deterministic. There are several

ways deterministic forcing can be implemented in an actual simulation. Linear forcing, which is discussed by Lundgren[5] for the incompressible case, assumes a forcing term in the momentum equations that is proportional to the velocity. In this case, the forcing term becomes similar to the natural production mechanism in the turbulent kinetic energy equation $\langle \mathbf{u}' \cdot \nabla \overline{\mathbf{u}} \cdot \mathbf{u}' \rangle$, where $\mathbf{u}'$ are the velocity fluctuations and the mean velocity gradient $\nabla \overline{\mathbf{u}}$ is assumed to be constant.

Typically, isotropic turbulence simulations are forced at low wavenumbers. The reasoning is that the dynamics of the inertial range at higher wavenumbers should evolve naturally, and not be influenced by the details of the forcing.[1,6] There are numerous studies of forced isotropic incompressible turbulence. Most of such investigations use spectral numerical methods and periodic domains, so restricting the linear forcing to low wavenumbers is convenient and efficient. In this case, the linear forcing term in the momentum equations becomes $\hat{\mathbf{f}}(\mathbf{k}) = c\hat{\mathbf{u}}(\mathbf{k})$ with $c=0$ when $k=|\mathbf{k}| \geq k_f$, where $\mathbf{u}$ is the velocity and $k_f=2.5$ is a common value. The coefficient may be chosen so that a constant kinetic energy K is maintained at the low wavenumbers,[7–9] or so that the energy injection rate is constant, $c = \epsilon/2K$.[1,10–12] The later has the advantage of being able to specify the dissipation ϵ, so that the Kolmogorov scale $\eta = (\nu^3/\epsilon)^{1/4}$ may be chosen at the onset for a well-resolved simulation.[10]

Low wavenumber (low-k) forcing is difficult to implement in domains with nonperiodic boundaries and is less convenient with nonspectral numerical methods. Lundgren[5] and Rosales and Meneveau[13] advocate linear forcing using the full spectrum velocity $\mathbf{f} = c\mathbf{u}$, which is simple to implement and efficient for physically based codes and can be

a)Electronic mail: mpetersen@lanl.gov.
b)Electronic mail: livescu@lanl.gov.

applied in any domain. For homogeneous isotropic incompressible turbulence, the full spectrum and low-k forcing produce substantial differences in high-order statistics at similar numerical resolutions. When compared with decaying grid turbulence experiments, full spectrum forced simulations exhibit a closer rate of approach to the 4/5-law than low-k forcing at similar Reynolds numbers.[14] Nevertheless, it should be noted that forced turbulence simulations are not intended to reproduce decaying turbulence experiments, but to probe high Reynolds number asymptotics with the resolutions possible on today's computers.

Unlike the extensive literature in incompressible turbulence, there are only a handful of studies of forced isotropic compressible turbulence. The theory of compressible isotropic turbulence significantly lags that of the incompressible case. For example, there is no generally accepted behavior of the inertial range and no analytical result regarding structure functions, analogous to the 4/5-law. In addition, even at subsonic turbulent Mach numbers, the turbulence develops shocklets—localized, short lived shock waves—which may change the dissipation properties, and thus the intermittency and the overall dynamics.[15,16] Compressibility effects are usually studied in high speed flows, but they may also arise in low speed flows when there is a mechanism for enhancing the dilatational (curl free) motions. This happens, for example, in turbulent combustion, where the heat release produces localized expansions and contractions.[17] In certain cases, the Mach waves associated to these dilatational motions can coalesce and lead to detonation. A similar result is obtained if the heat release is large enough so that the flow is locally accelerated to supersonic velocities. In such flows, the dilatational motions can carry a significant amount of energy compared to the incompressible (solenoidal or divergence free) motions.

Several studies of forced compressible turbulence follow the stochastic methods of Eswaran and Pope[2,18–21] or Kida and Orszag.[22–24] Those using deterministic forcing have only used fixed fields: e.g., three orthogonal shear waves at $k=1$ (Ref. 25) or simply the initial velocity field.[26] In this case, the imprint of initial conditions or that of the (fixed) forcing fields may have a long lasting influence and one needs to perform many different realizations to reduce the statistical variability.

Due to the advantages of the linear forcing (both full spectrum and the low-k restriction) and, arguably, general acceptance for the incompressible case, the purpose of this paper is to discuss the extension of such forcing to the compressible case. It is shown that, unlike the incompressible case, two independent coefficients are required for compressible turbulence simulations, which set the solenoidal and dilatational parts of the forcing separately. In addition, since a solenoidal-dilatational decomposition of the velocity field is required for the forcing, the simplicity of the full spectrum linear forcing implementation in physical-space numerical codes is lost.

The linear forcing studied here is a particular instance of the generalized formula: $f_i = A_{ij} u_j$. Other types of forcing encompassed by this formula include anisotropic forcing, such as homogeneous shear flow,[27,28] plane strain,[27] or axisymmetric contraction,[27,29] as well as isotropic strain,[27,29] which can be compression or expansion. Isotropic compression forcing has a similar expression to that used here, the main difference being that the coefficients A_{ij} satisfy the mean momentum equation, which constrains the maximum duration of the simulation. The resulting flows have been studied extensively for the compressible case, but only during the growth stage, before statistical stationarity has been reached. In all flows studied under linear forcing in the generalized sense, the main compressibility effect during the evolving stage is to reduce the growth of the turbulence fluctuations. Although compressibility reduces the turbulence production,[30] it appears that direct changes to the pressure field are mainly responsible for the reduction of the turbulence growth. Thus, for the homogeneous shear flow, the turbulent kinetic energy decreases with the Mach number in the rapid distortion theory limit even though the energy production approaches a constant independent of the Mach number.[31] The analytical solutions derived by Livescu and Madnia[28] clearly indicate the linear mechanism through which compressibility affects the growth of anisotropic linearly forced turbulence. In addition, nonstationary linearly forced turbulence generally has larger levels of explicit dilatational effects (e.g., the magnitude of the pressure-dilatation correlation and the dilatation to solenoidal dissipation ratio) than some basic nonreacting inhomogeneous compressible flows, such as high speed boundary or mixing layers,[32–34] where the forcing is not linear due to the spatial variation of the mean velocity gradient. Although the origin of this difference is still an open problem, we note that the rapid distortion theory can be used to highlight the connection between the forcing and the explicit dilatational effects.[28] Here, we show that in the stationary state, the amplification of the dilatational effects becomes even more dramatic, with the probable asymptotic state corresponding to the kinetic energy residing entirely in the dilatational component. Consequently, in order to be able to control the late time state, two separate forcing terms are required. The ability to explicitly control the magnitude of the dilatational effects may also allow studies relevant to both types of compressible flow situation mentioned above.

Previous studies of forced compressible turbulence used forcing terms based on the velocity. In principle, one can add a forcing term that depends on the thermodynamic state, corresponding to entropy mode fluctuations. For example, the linear forcing implied by the advection term in the internal energy equation is ce, where c is a constant depending on the mean velocity gradient. Then, to conserve the total energy, a term $-ce$ needs to be added to the kinetic energy equation. However, such a form is not appropriate for the momentum equations, as it requires a division by velocity. In addition, the forcing term used in the paper, while it depends only on the velocity field, clearly also excites the entropy mode, since it is present in the internal energy equation as $-f_i u_i$ (see below).

The paper is organized as follows. Section II describes the governing equations and numerical methodology, Sec. III discusses the extension of the linear forcing to the compressible case, and Sec. IV compares the full spectrum to low-k

forcing. In order to assert the need for multiple realizations, Sec. V compares the computational requirements for performing single versus ensemble realizations. Finally, a summary and conclusions are presented in Sec. VI and a brief overview of the resolution requirements for the physical-space compact finite differences method used here, which is compared to the usual spectral differencing, is given in the Appendix.

II. GOVERNING EQUATIONS AND NUMERICAL METHOD

A compressible, ideal fluid flow is governed by continuity, momentum, and energy transport equations. In nondimensional form, these equations are[17]

$$\frac{\partial \rho}{\partial t} + (\rho u_j)_{,j} = 0, \tag{1}$$

$$\frac{\partial \rho u_i}{\partial t} + (\rho u_i u_j)_{,j} = -p_{,i} + \tau_{ij,j} + f_i, \tag{2}$$

$$\frac{\partial \rho E}{\partial t} + (\rho E u_j)_{,j} = -(u_j p)_{,j} + (u_i \tau_{ij})_{,j} - q_{j,j} + f_j u_j + f_e, \tag{3}$$

where f_i and f_e are forcing terms on the momentum and internal energy equations. The primary dependent variables are the density ρ, the velocity components in directions $i = 1, 2, 3, u_i$, and the specific total energy $E = h + u_i u_i / 2 - p / \rho$, where h is the specific enthalpy and p is the pressure. Equations (1)–(3) are nondimensionalized using reference values for density ρ_0, velocity u_0, length, L_0, time $t_0 = L_0 / u_0$, temperature T_0, and molecular transport properties as defined below.

The stress tensor is Newtonian, $\tau_{ij} = \mu / \mathrm{Re}_0 [(u_{i,j} + u_{j,i}) - 2/3 u_{m,m} \delta_{ij}]$, where μ is the dynamic viscosity and Stokes' hypothesis is assumed valid, δ_{ij} is the Kronecker delta, and $\mathrm{Re}_0 = \rho_0 u_0 L_0 / \mu_0$ is the computational Reynolds number, with μ_0 the reference value for viscosity. The dynamic viscosity is temperature dependent, $\mu = T^{0.76}$. The temperature T is nondimensionalized by T_0, the pressure by $\rho_0 u_0^2$, and the specific energy and enthalpy by u_0^2. Thus, the pressure and caloric equations of state become

$$p = \frac{\rho T}{M_0^2}, \tag{4}$$

$$h = \frac{\gamma T}{(\gamma - 1) M_0^2}, \tag{5}$$

where M_0 is the reference Mach number (see below) and γ is the ratio of specific heats. The heat flux obeys Fourier's law $q_j = -\gamma \lambda_c / (\gamma - 1) M_0^2 \mathrm{Pr} \mathrm{Re}_0 T_{,j}$ with the conduction coefficient taken to have the same variation with the temperature as the viscosity, $\lambda_c = T^{0.76}$. The reference velocity is chosen such that the initial turbulent kinetic energy is 0.5, $\rho_0 = 1$, and L_0 is the size of the computational box for all simulations.

In general, the influences of the ratio of specific heats and the Mach number based on the isothermal sound speed are different.[35–37] To highlight this difference, the computa-

TABLE I. Parameter values of simulations, where series 1 was used for long-time simulations on a 128^3 mesh (Figs. 1–6) and series 2 was used for high-resolution simulations on a 1024^3 mesh (Figs. 5–10). All simulations use Pr=1 and γ=1.4. For the split forcing described below, the initial values of M_t and target ϵ_d / ϵ_s are close to their values in the stationary state.

Name	Series 1				Series 2			
	1a	1b	1c	1d	2a	2b	2c	2d
M_t	0.02	0.1	0.3	0.3	0.1	0.1	0.3	0.3
ϵ_d / ϵ_s	0.1	0.1	0.3	1.0	0.033	0.3	0.1	0.3

tional Mach number M_0 is defined in the formulas above based on the reference isothermal sound speed, $c_0 = \sqrt{RT_0}$, where R is the gas constant.

The forcing terms f_i and f_e are described in Sec. III. Extensions to inhomogeneous flows are possible, but here we restrict the discussion to periodic domains and homogeneous flows. Thus, the averages are calculated as volume and time averages after the stationary state is reached. Below, the volume average of the variable f is denoted by $\langle f \rangle$ and the volume and time average is denoted by $\langle f \rangle_{\mathrm{equil}}$.

The terms solenoidal and dilatational are frequently used in this paper and are defined as follows. Given a three-dimensional vector field $\mathbf{u}$, there exists a decomposition (usually called Helmholtz or Weyl decomposition) $\mathbf{u} = \mathbf{u_s} + \mathbf{u_d}$ where $\nabla \times \mathbf{u_d} = 0$ and $\nabla \cdot \mathbf{u_s} = 0$.[22,38] For periodic domains, the Helmholtz-Weyl decomposition is unique up to a constant. If $\mathbf{u}$ is the velocity field, the constant can be taken equal to zero without loss of generality, as the equations are invariant to a constant translational velocity. The two contributions $\mathbf{u_s}$ and $\mathbf{u_d}$ are usually called the solenoidal and dilatational components, but are sometimes referred to as the rotational and compressible components.

Equations (1)–(3) are solved in real space with the CFDNS code,[39] using sixth-order compact finite differences for spatial derivatives,[40] and the variable time step fourth-order Runge–Kutta–Fehlsberg method for time integration. The simulations were conducted on up to 1024^3 meshes for a range of values of Re_0, M_0, γ, ϵ_d / ϵ_s, and Pr. The bulk of these results will be discussed in a separate paper. Here, we restrict the discussion to the properties of the forcing terms and all results presented were obtained with Pr=1 and γ =1.4. The simulations achieve Taylor Reynolds numbers $\mathrm{Re}_\lambda = \mathrm{Re}_0 u_{\mathrm{rms}} \lambda / \nu$ of up to 300, and cover the range of turbulent Mach numbers $M_t = 0.02 - 0.3$ and $\epsilon_d / \epsilon_s = 0.0 - 1.0$. Table I lists the parameter values of simulations shown in the plots. Here, $u_{\mathrm{rms}} = \sqrt{\langle u_i u_i \rangle / 3}$, $\lambda = u_{\mathrm{rms}} / \sqrt{\langle u_{i,i}^2 \rangle / 3}$, $\nu = \langle \mu \rangle / \langle \rho \rangle$, and the turbulent Mach number is defined as $M_t = M_0 \langle u_i u_i \rangle^{1/2} / (\gamma \langle T \rangle)^{1/2}$, where $(\gamma \langle T \rangle)^{1/2}$ is the volume-averaged speed of sound for the nondimensionalization considered.

The variables are initialized with zero dilatational velocity and density fluctuations. The solenoidal velocity is initialized as a random Gaussian field with an approximate Kolmogorov spectrum and turbulent kinetic energy of 0.5. The initial pressure fluctuations are determined from the Poisson equation $p_{,kk} = -(u_i u_j)_{,ij}$, and the mean pressure is

adjusted to obtain the desired initial turbulent Mach number. The temperature and specific energy are then calculated from the equations of state. In order to test the influence of initial conditions, the dilatational field was also initialized following Ristorcelli and Blaisdell.[41] Although the initial conditions have a long lasting influence on the development of decaying turbulence,[42] we found no difference in the adjustment time or equilibrium statistics of the simulation for the forced case. All simulations were well resolved in the stationary regime. The criterion used is based on a Fourier analysis of the error for the sixth order compact scheme (see below) corresponding to $\eta k_{max} = 1.5$ in a spectral simulation and was verified through resolution studies. The simulations were also monitored to ensure that the shocklets, which increase in number and strength as M_t and ϵ_d/ϵ_s increase, remain well resolved. To reduce the computational effort for the adjustment time, the runs were started with half the resolution and then interpolated to the final resolution once the statistics approached stationarity. The procedure was verified to yield identical results compared to a complete run at full resolution.

III. LINEAR FORCING FOR STATIONARY COMPRESSIBLE ISOTROPIC SIMULATION

The volume average of Eq. (3), $d/dt\langle \rho E \rangle = \langle f_j u_j \rangle + \langle f_e \rangle$, shows that setting $f_e = -f_j u_j$ ensures that the total energy is conserved. Note that f_e is the forcing term in the transport equation for the internal energy, $\rho e = \rho h - p$. This choice of f_e ensures that the internal energy (and the temperature) can reach a stationary state.

The volume-averaged kinetic energy equation is

$$\frac{dK}{dt} = -\langle u_i p_{,i} \rangle - \epsilon + \langle u_i f_i \rangle, \tag{6}$$

where $K = \langle \rho u_i^2 \rangle / 2$ and the dissipation $\epsilon = -\langle u_i \tau_{ij,j} \rangle$. The forcing investigated here is a simple linear forcing[5,13]

$$f_i = c\rho u_i, \tag{7}$$

where c is constant throughout the domain [the low-k case with $c = c(\mathbf{k})$ is similar], but may change in time.

Then, at the equilibrium

$$(2cK - \epsilon + PD)_{equil} = 0. \tag{8}$$

where $PD = -\langle u_i p_{,i} \rangle = \langle u_{i,i} p \rangle$ is the pressure-dilatation correlation (the last equality is a consequence of homogeneity). In Eq. (8), one can specify either the coefficient c or use the instantaneous values for either ϵ or PD, or both, in which case c is time dependent. We found that Eq. (7) is not sufficient for compressible flows since there is no mechanism to control the ratio of dilatational to solenoidal kinetic energies. For a single forcing term, the probable long time state corresponds to the kinetic energy residing entirely in the dilatational component. To clarify this point, we consider separately the solenoidal and dilatational kinetic energy transport equations,

$$\frac{1}{2}\frac{d\langle w_{i_\alpha}^2 \rangle}{dt} = \left\langle -(w_i u_j)_{,j} w_{i_\alpha} + \frac{1}{2} w_i u_{j,j} w_{i_\alpha} \right\rangle - \left\langle p_{,i} \frac{w_{i_\alpha}}{\sqrt{\rho}} \right\rangle$$
$$+ \left\langle \tau_{ij,j} \frac{w_{i_\alpha}}{\sqrt{\rho}} \right\rangle + \left\langle f_i \frac{w_{i_\alpha}}{\sqrt{\rho}} \right\rangle. \tag{9}$$

These equations are obtained by dotting the transport equation for $\sqrt{\rho}u_i$, which is derived from Eqs. (1) and (2), with w_{i_α} and averaging over the domain.[17,22] Here $w_{i_\alpha} \equiv (\sqrt{\rho}u_i)_\alpha$ and α may designate the solenoidal (s), dilatational (d), or average (o) components. Since there is no directionality in this flow and the mean velocity is assumed zero, flux quantities such as $\langle \sqrt{\rho}u_i \rangle$ are zero.[17,43] Assuming that the contributions from the advective terms and the pressure dilatation contribution to the solenoidal kinetic energy equation are small, it yields

$$\frac{dK_s}{dt} = -\epsilon_s + \left\langle f_i \frac{w_{i_s}}{\sqrt{\rho}} \right\rangle, \tag{10}$$

$$\frac{dK_d}{dt} = PD - \epsilon_d + \left\langle f_i \frac{w_{i_d}}{\sqrt{\rho}} \right\rangle. \tag{11}$$

Setting the time derivative to zero, $f_i = c\rho u_i$ with c constant, and noting that $\langle w_i w_{i_\alpha} \rangle = \langle w_{i_\alpha} w_{i_\alpha} \rangle = 2K_\alpha$ in the stationary regime one obtains

$$\epsilon_{s_{equil}} = 2cK_{s_{equil}}, \tag{12}$$

$$\epsilon_{d_{equil}} = PD_{equil} + 2cK_{d_{equil}}. \tag{13}$$

Since c and the dissipation parts are positive at equilibrium, the pressure dilatation needs to be bounded by $-\epsilon_{s_{equil}} K_{d_{equil}} / K_{s_{equil}} \le PD_{equil} \le \epsilon_{d_{equil}}$. It is known that PD oscillates significantly in time even when the average is small,[17,32,43] which is a direct consequence of the dynamics of the sound waves generated by and interacting with the turbulence. The magnitude of the oscillations increases with the pressure, so they become larger at small turbulent Mach numbers. When PD takes positive values larger than the current time average, the dilatational kinetic energy increases, further amplifying PD. The dilatational dissipation also increases, and if this change is smaller or comparable to that of PD, a new equilibrium is reached at higher levels of dilatational kinetic energy. However, when PD takes negative values smaller than the current time average, K_d decreases, which tends to reduce the magnitude of the negative PD value. Thus, the dynamical equations (10) and (11) tend to bias PD toward large positive values and the tendency should be more pronounced at smaller turbulent Mach numbers. In addition, a bias toward large PD values also leads to a decrease in the solenoidal kinetic energy. If the instantaneous PD is used in Eq. (8), this directly affects the equilibrium state in the Eq. (10). If a constant value is used for PD in Eq. (8), note that only one of the PD and ϵ values can be specified or the difference, but not both, and the problem becomes similar. Therefore, larger equilibrium values for PD lead to larger dilatational to solenoidal dissipation and kinetic energy ratios and the only stable equilibrium seems to corre-
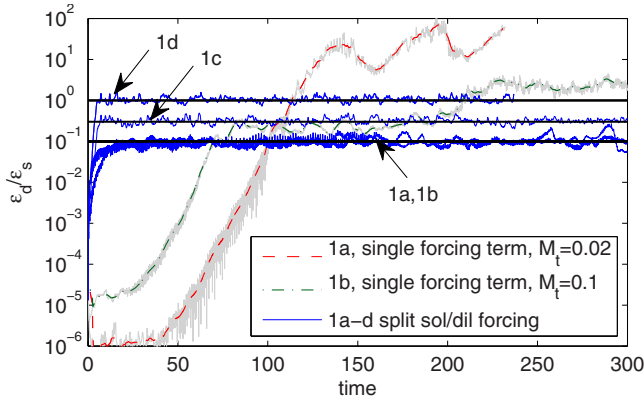
FIG. 1. (Color online) Evolution of ϵ_d/ϵ_s, which is the dilatational to solenoidal dissipation ratio, for unsplit and split forcing. When a single forcing term is used [Eq. (7)] there is no control over ϵ_d/ϵ_s, and it often continues to grow throughout the simulation. With a split solenoidal/dilatational forcing [Eq. (17)] ϵ_d/ϵ_s quickly adjusts to the imposed value (solid horizontal lines). For clarity, single forcing term data are averaged over a 5 s window. The light gray is unaveraged data, and shows high variability in the single term forcing results.

spond to ϵ_d/ϵ_s and K_d/K_s approaching infinity, when almost all kinetic energy is dilatational. Our numerical tests verify this conjecture (see Figs. 1 and 2). The evolution of K_d/K_s exhibits short intervals at quasiequilibrium then jumps to higher values as large instantaneous PD values, which are allowed by its variability, move the equilibrium to higher K_d/K_s. At higher turbulent Mach numbers, PD variability decreases and the equilibrium becomes more stable; however, long time readjustments cannot be ruled out. The increase in ϵ_d/ϵ_s and K_d/K_s with time for a single forcing term also translates in an increase in the total dissipation and turbulent kinetic energy, mainly due to the dilatational contribution (see Figs. 3 and 4), as well as an increase in the turbulent Mach number. Nevertheless, the variation of M_t does not follow a linear relation with respect to the ratio ϵ_d/ϵ_s. In fact, the single forcing term prevents the flow from reaching acoustic equilibrium as in decaying isotropic compressible turbulence.[44]

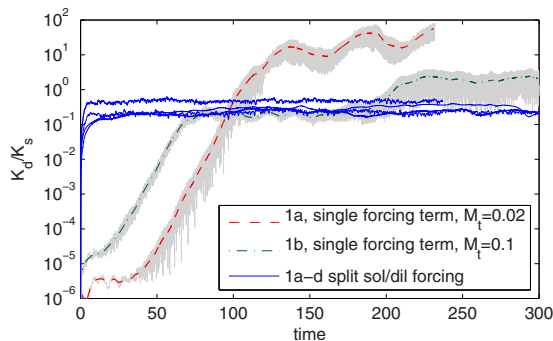These difficulties can be avoided by forcing the solenoidal and dilatational velocities separately,

FIG. 2. (Color online) The ratio of dilatational to solenoidal kinetic energy K_d/K_s reaches the equilibrium value about the same time as ϵ_d/ϵ_s; however, the specific value is different than ϵ_d/ϵ_s and depends on the turbulent Mach number.
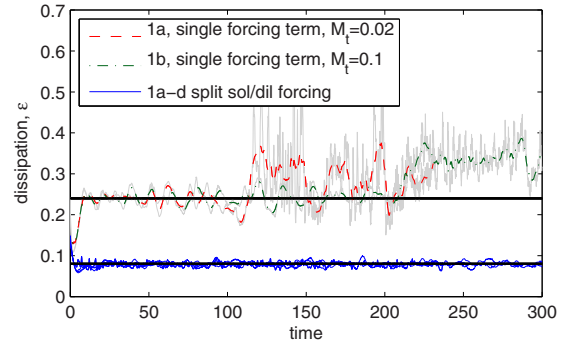

FIG. 3. (Color online) Evolution of the total dissipation for unsplit and split forcing. The forcing coefficients can be cast in a form that allows the specification of the dissipation (solid horizontal lines) and, thus, the Kolmogorov microscale. The split forcing method adheres closely to the imposed dissipation (solid horizontal lines) unlike the single term forcing method.

$$f_i = c_s\sqrt{\rho}w_{i_s} + c_d\sqrt{\rho}w_{i_d}. \tag{14}$$

Substituting into Eqs. (10) and (11), and noting that $\langle w_{i_s}w_{i_d}\rangle=0$, the two coefficients take the following forms:

$$c_s = \frac{\epsilon_{s\ target}}{2K_s}, \tag{15}$$

$$c_d = \frac{\epsilon_{d\ target} - PD}{2K_d}. \tag{16}$$

Equivalently, one may specify the dissipation ratio ϵ_d/ϵ_s and the total dissipation ϵ (Figs. 1 and 3). The ability to specify ϵ allows the control of the Kolmogorov scale, $\eta=(\nu^3/\epsilon)^{1/4}$, so that the simulation may be well-resolved. Note that if the forcing coefficients are chosen to control ϵ_d/ϵ_s, the ratio of dilatational to solenoidal kinetic energies K_d/K_s may, in general, be different than ϵ_d/ϵ_s, depending on the turbulent Mach number (Fig. 2).

For split forcing, the values of M_t and ϵ_d/ϵ_s can be fixed at the onset. Thus, the flow does reach equilibria among various kinetic and integral energy components, and the proportionality constants can be adjusted to any value. Therefore,
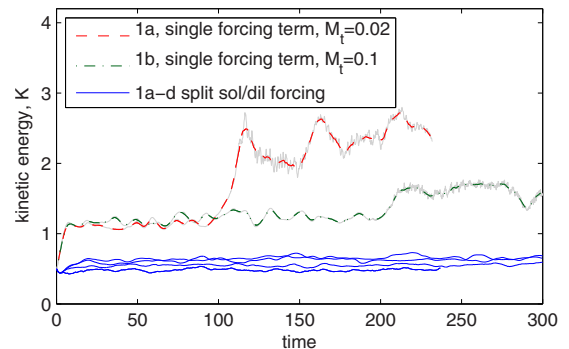

FIG. 4. (Color online) Time variation of the turbulent kinetic energy for unsplit and split forcing. The increase in K_d/K_s for unsplit forcing causes the turbulent kinetic energy to increase as well.

by appropriately choosing the forcing properties, the equilibrium state can be "designed" to be similar to various practical flows, which allow the study of compressible turbulence in diverse regimes.

IV. FULL SPECTRUM VERSUS LOW WAVENUMBER FORCING

For the incompressible case, Lundgren[5] argues that the full spectrum linear forcing is preferable to its restriction to low wavenumbers since the approach to the 4/5 law is closer to that obtained in decaying grid turbulence experiments at similar Reynolds numbers. In addition, it obviates the expense of Fourier transforms in simulations using real-space numerical codes.[13] Nevertheless, low wavenumber forcing (or filtered forcing) allows higher Reynolds numbers to be reached and adds little or no energy to higher wavenumbers, while full spectrum forcing achieves lower Reynolds numbers and adds energy throughout the spectrum.[5] For compressible turbulence simulations, separate solenoidal and dilatational forcing components are needed to run stably and the decomposition of the velocity field requires Fourier transforms or Poisson solvers. Thus the advantage of full spectrum linear forcing in real-space numerical codes is lost. It is shown below that restricting the linear forcing to low wavenumbers is actually more computationally efficient for compressible turbulence calculations using real-space codes.

We now proceed to a comparison of full spectrum linear forcing versus low-k forcing for the compressible case. The later may be written in the split dilatational/solenoidal formulation as

$$f_i = c_s \sqrt{\rho} \widetilde{w}_{i_s} + c_d \sqrt{\rho} \widetilde{w}_{i_d}, \tag{17}$$

$$c_s = \frac{\epsilon_{s\ \text{target}}}{\langle \widetilde{w}_{i_s} w_i \rangle}, \tag{18}$$

$$c_d = \frac{\epsilon_{d\ \text{target}} + \langle u_i p_{,i} \rangle}{\langle \widetilde{w}_{i_d} w_i \rangle}, \tag{19}$$

where the spectrally filtered modified velocity $\widetilde{w}_{i_\beta}$ ($\beta = s$ for solenoidal or d for dilatational) is found by computing the Fourier coefficients $\hat{w}_i(\mathbf{k})$ for $|\mathbf{k}| < k_0$ (e.g., $k_0 = 1.5$ corresponds to 18 modes in three-dimensional). Dilatational and solenoidal components of the velocity field must be computed in Fourier space as[38]

$$\hat{w}_{i_d}(\mathbf{k}) = k_i (\mathbf{k} \cdot \hat{w})/|\mathbf{k}|^2, \tag{20}$$

$$\hat{w}_{i_s}(\mathbf{k}) = \hat{w}_i(\mathbf{k}) - \hat{w}_{i_d}(\mathbf{k}). \tag{21}$$

For the case of low wavenumber forcing, the full Fourier transform may be avoided by reassembling the coefficients with a small inverse transform,

$$\widetilde{w}_{i_\alpha}(\mathbf{x}) = \sum_{\mathbf{k}} \hat{w}_{i_\alpha}(\mathbf{k}) e^{-2\pi i \mathbf{k} \cdot x}, \quad |\mathbf{k}| < 1.5. \tag{22}$$

The forcing term in the momentum equations has mean zero ($\hat{w}_{i_\alpha}(\mathbf{0}) = 0$), which is a requirement for stable forcing. Note that $\langle \widetilde{w}_{i_\alpha} w_i \rangle = \langle \widetilde{w}_{i_\alpha} w_{i_\alpha} \rangle$, and the choice of $\langle \widetilde{w}_{i_\alpha} w_i \rangle$ in the de-

TABLE II. Low-k forcing achieves nearly double the Taylor Reynolds number as that of full spectrum forcing at the same resolution with the same ηk_{max} criterion for all runs.

Resolution	128^3	256^3	1024^3
R_λ, full forcing	35	55	
R_λ, low-k forcing	60	100	300

nominators of Eqs. (18) and (19) avoids the need to compute w_{i_α}.

A major advantage of low-k forcing is that the Taylor Reynolds number is much larger than that obtained with full spectrum forcing. For example, for the simulations presented here, Re$_\lambda$ is nearly double for low-k forcing (Table II). At a fixed resolution, the Taylor microscale λ is 30% larger, and the kinetic energy is 70% larger for low-k forcing even though the average dissipation is the same for both methods. The larger kinetic energy is due to the high energy content at small wavenumbers.

In low-k forcing, the injection scale and dissipation scale are separated, so that an inertial range, which is unaffected by the large scale forcing and dissipation, can develop. This can be seen in the energy flux $\Pi(k)$, a variation with the wavenumber. Thus, $\Pi(k) + PD$ is equal to the full dissipation (and forcing) for a range of wavenumbers just above the forcing range (Fig. 5, see Ref. 3 for definitions and similar plots). In contrast, the full spectrum linear forcing, which has a spectrum proportional to that of the kinetic energy itself, affects higher wavenumbers and requires much larger Reynolds numbers so that the forcing magnitude decreases enough for an inertial range to develop. For the compressible case, the pressure dilatation, which transfers energy between kinetic and internal energies, may also play a role in the overall energy balance, especially when the dilatational energy is large. The question of how this affects the inertial range dynamics will be addressed in a future paper. We now note that its contribution was added together to the transfer function in order to recover the dissipation and forcing values.

An inertial range can develop in full spectrum linearly forced simulations at scales where the production and dissi-
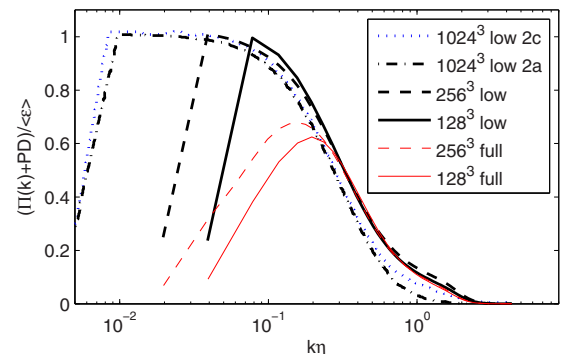

FIG. 5. (Color online) The energy flux is equal to the dissipation for a range of wavenumbers for low-k forcing but not for full spectrum linear forcing, which requires larger resolutions to develop an inertial range. The results correspond to the parameters from run 1c except as noted.
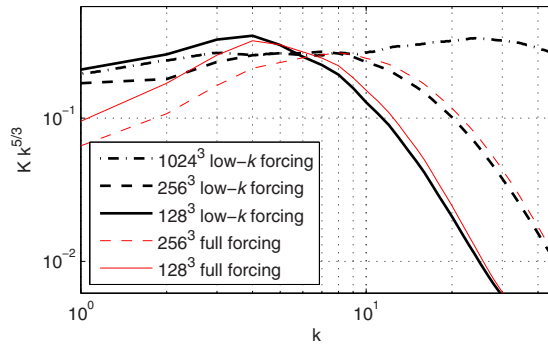
FIG. 6. (Color online) The energy content at low wavenumbers is lower when full spectrum linear forcing is used, compared to low-k forcing, which results in a lower overall Reynolds number. The results correspond to the parameters from run 1c.

pation terms in the spectral kinetic energy balance are small. However, for the full spectrum linear forcing, the forcing term has a lingering effect at high wavenumbers and simple scaling arguments can be made to show that the dissipation and the scales affected by forcing overlap at 1024^3 resolutions. In addition, the energy content at low wavenumbers is lower for full spectrum compared to low-k forcing (Fig. 6), resulting in an overall lower Reynolds number (Table II). On the other hand, if the low-k restriction of the linear forcing is used, an inertial range develops in 1024^3 simulations (Fig. 7). Figures 7(b) and 7(c) also show that the spectral characteristics are different for the solenoidal and dilatational parts of the kinetic energy. Thus, the solenoidal kinetic energy spectrum decays close to the incompressible value of $-5/3$, while the dilatational kinetic energy spectrum is steeper.

One of the few exact results concerning incompressible turbulence is the 4/5 law, which states that the peak normalized value of the third-order longitudinal structure function should approach 0.8 in the limit of high Reynolds number. The rate of approach to the asymptotic value is faster in low-k forcing,[45] while full spectrum linear forcing yields a rate of approach closer to that obtained in decaying grid turbulence experiments.[5,14] The split forcing method described here produces these same trends for the compressible case (Fig. 8).

Although the structure function laws are derived under the assumption of incompressibility, we check how the so-called 4/15, 4/5, and 4/3 laws are satisfied near the incompressible limit, simulation 2a with low M_t and ϵ_d/ϵ_s, which reaches a Taylor Reynolds number of 300. The split low-k forcing produces structure functions that peak close to the incompressible values (Fig. 9). For example, $-D_{LLL}/(\bar{\epsilon}r)$ peaks at 0.774, which is consistent with the incompressible results at the same Reynolds number presented by Kaneda et al.[45] The third-order isotropy relation is also consistent with incompressible simulations[3,46] (Fig. 10). Here

$$D_{LLL} = \langle(\delta u_L)^3\rangle_{\text{equil}}, \tag{23}$$

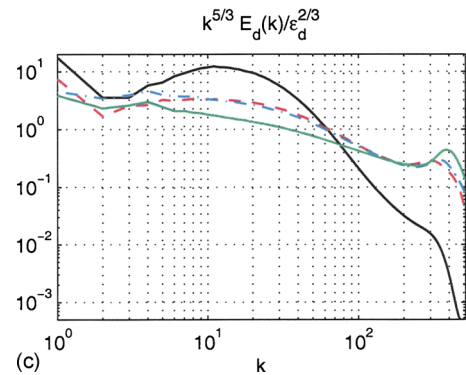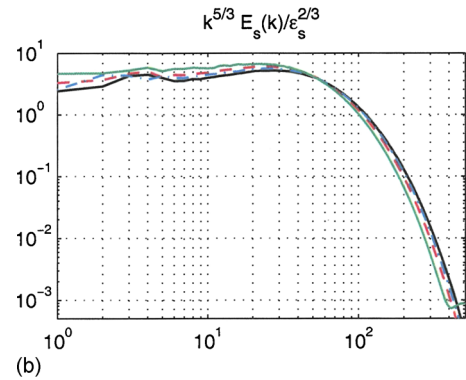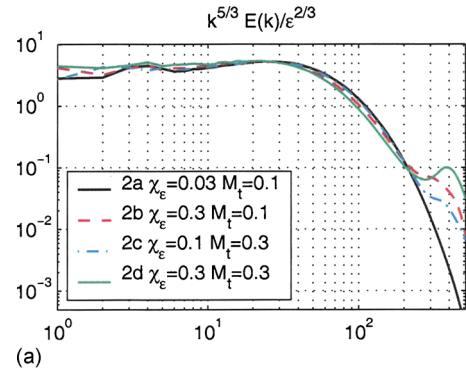$$D_{LTT} = \langle\delta u_L(\delta u_T)^2\rangle_{\text{equil}}, \tag{24}$$

FIG. 7. (Color online) Compensated kinetic energy spectra obtained from 1024^3 low-k split forced simulations at different M_t and ϵ_d/ϵ_s values: (a) total kinetic energy, (b) solenoidal, and (c) dilatational parts of the kinetic energy.

$$\delta u_L(\mathbf{r},\mathbf{x}) = [\mathbf{u}(\mathbf{x}+\mathbf{r}) - u(\mathbf{x})]\cdot\hat{\mathbf{r}}, \tag{25}$$

$\hat{\mathbf{r}}=\mathbf{r}/r$ and δu_T is a velocity increment along a vector transverse to the separation vector $\mathbf{r}$. To compute structure functions we use the method of Taylor et al.,[46] which angle-averages over 73 directions in order to obtain a large number of samples from a reduced set of instantaneous data fields.

V. SINGLE VERSUS ENSEMBLE REALIZATIONS

In collecting long-time averages of statistics, one would like to know if it is more efficient to run a single simulation for a long time, or an ensemble of simulations each for a shorter time. Since this forcing method sets a target value for ϵ and ϵ_d/ϵ_s, we may measure the error from a single simulation as
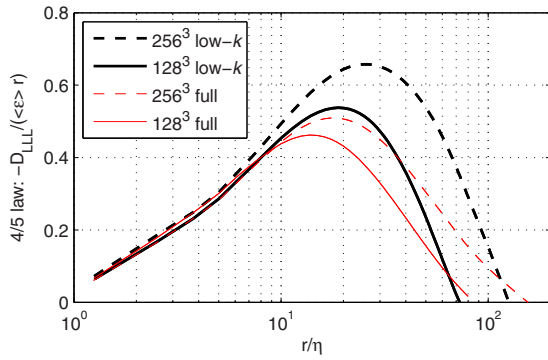
FIG. 8. (Color online) Third-order structure function $-D_{LLL}/(\bar{\epsilon}r)$ from low-wavenumber split linear forcing (thick lines, black on-line) and full spectrum split linear forcing (thin lines, red on-line) for series 1c. At a particular resolution, low-k forcing produces a higher peak than full spectrum forcing.

$$e(T) = \frac{\bar{x}(T) - x_{\text{equil}}}{x_{\text{equil}}} \tag{26}$$

and from the ensemble as

$$E(T) = \frac{\sum_{i=1}^{n} \bar{x}_i(T)/n - x_{\text{equil}}}{x_{\text{equil}}}, \tag{27}$$

where x_{equil} is the average (target value) of quantity x and $\bar{x}(T) = 1/T \int_{t_0}^{t_0+T} \langle x \rangle(t) dt$ is the average of x using a finite time T. The subscript represents each of n realizations and t_0 is the initial adjustment time.

To compare single realization versus ensemble averaging, we considered three realizations of a 256^3 simulation that differed only in the random number seed for the initial condition. Time averages were computed from $t_0 = 10$ s onward, so that the initial large adjustment does not affect the average.

Figure 11 plots the error for each realization and the ensemble, as a function of model time (which includes the
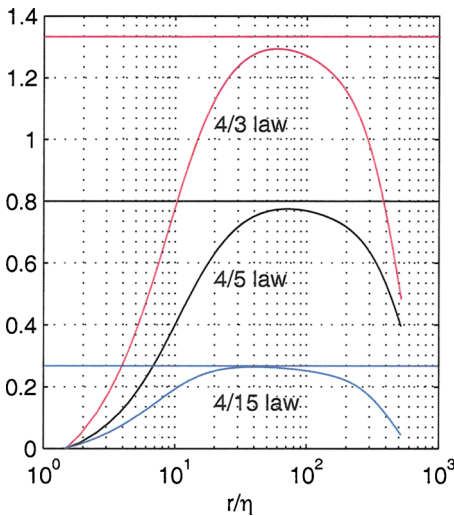

FIG. 10. (Color online) Isotropy relation at third order for simulation 2a, with 1024^3 grid cells and $R_\lambda = 300$ using low-k split forcing. Solid line (red on-line): D_{LTT}/r, dashed line (blue on-line): $(d/dr)(rD_{LLL})/(6r)$.

initial adjustment time) required to obtain that average. For the ensemble of three runs, 30 s of model time are required to get past the initial adjustment and begin computing averages. This amount of time weighs significantly on the final computational price. For any investment of computing time, the ensemble average error is always greater than the error from a single realization. In other words, it is better to com-

(a)

(b)

FIG. 11. Error in average statistics when using separately each of three realizations (thin lines) or the average of the three (thick line). The horizontal axis is the total model time required to compute the average. This comparison shows that computing time is better spent measuring statistics over one simulation, rather than taking the average of an ensemble of simulations.

FIG. 9. (Color online) Structure function curves for the high resolution, nearly incompressible simulation 2a, with 1024^3 grid cells and $R_\lambda = 300$, using low-k split forcing. All three curves peak near the theoretically expected values (horizontal lines). Bottom: 4/15 law, $-D_{LTT}/(\bar{\epsilon}r)$; middle: 4/5 law, $-D_{LLL}/(\bar{\epsilon}r)$; and top: 4/3 law, $-(D_{LLL}+2D_{LTT})/(\bar{\epsilon}r)$.
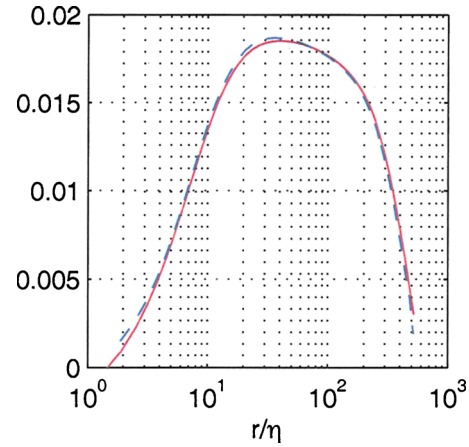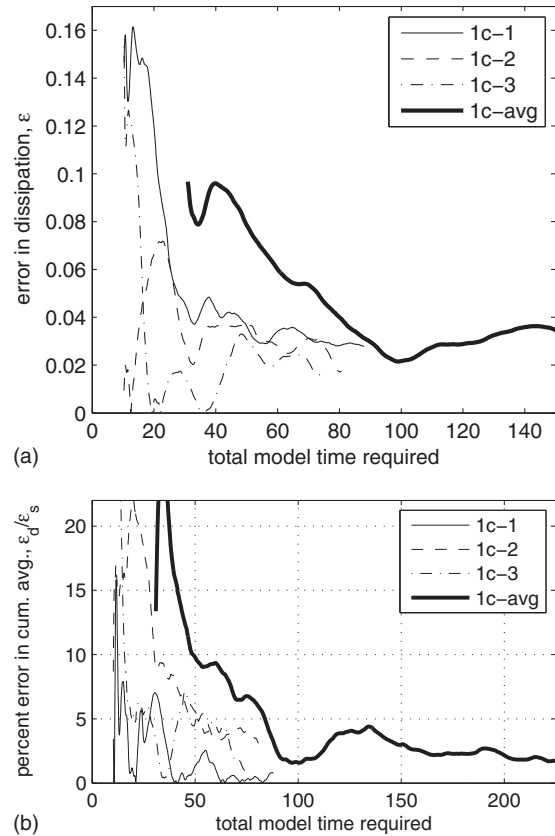
pute averages based on one simulation than an ensemble. The opposite would be true if the initial adjustment time was much shorter or if any single realization exhibited long range time correlations. Nevertheless, in this case, the forcing leads to rich variability of the large scales, which make multiple realizations unnecessary.

VI. CONCLUSIONS

Isotropic turbulence simulations provide an idealized configuration to study turbulence properties in detail without complications due to boundaries or inhomogeneities. This is also an ideal configuration to study high Reynolds number asymptotics. In order to reach the largest Reynolds numbers allowed by a given grid size, the turbulence needs to be sustained by an external stirring force. The linear forcing scheme studied by Lundgren[5] and Rosales and Meneveau[13] for incompressible turbulence is similar to the natural Reynolds shear stress production mechanism in the turbulent kinetic energy equation and also has a straightforward implementation in physical-space numerical codes. In order to increase the Reynolds number of the simulation and, thus, be able to probe inertial range dynamics and higher order turbulence statistics with today's computers, linear forcing can be restricted to low wavenumbers.[1]

Compared to the incompressible case, the theory of compressible turbulence lags significantly behind. Thus, it is not clear what the properties of the inertial range should be, nor there are analogous results, e.g., to the 4/5 law. Even less is known about higher order turbulence statistics. Compressibility effects in turbulence can appear in high speed or shocked flows and may be important for modeling supersonic aerodynamics. They can also appear in low speed flows in which there is a mechanism for enhancing the nondivergence free motions, e.g., exothermic reactions. Ramjets and cosmic explosions are examples where both situations occur. In turbulent combustion, the localized expansions due to the heat release can increase the local velocity to supersonic values and generate shocklets. In certain situations, these shocklets can coalesce and lead to detonation. Compressibility effects are thus characterized by the Mach number of the turbulent fluctuations, but also by the distribution of kinetic energy between the divergence free and curl free components of the velocity.

Since the linear forcing and its restriction to low wavenumbers have been successfully used for studying the characteristics of incompressible turbulence at high Reynolds numbers, this paper discusses extensions to the compressible case. It is shown that, unlike the incompressible case, a single linear forcing term leads to unstable simulations, in which the ratio of dilatational to solenoidal kinetic energies increases without bound. This is due to the large time variability of the pressure dilatation correlation, an effect that is stronger closer to the incompressible limit. The solution is to introduce two forcing terms that would separately force the solenoidal and dilatational components of the kinetic energy. In addition, the two independent forcing coefficients can be cast in a form that allows the control of the equilibrium

values of the total dissipation and the dilatational to solenoidal dissipation ratio. Thus, the equilibrium Kolmogorov microscale can be controlled from the onset.

Previous studies of homogeneous compressible turbulence with generalized linear forcing in nonstationary regimes (e.g., homogeneous shear or isotropic strain), found explicit dilatational effects larger than those present in some basic nonreacting inhomogeneous flows, such as compressible boundary or mixing layers, where the forcing is not linear. While the origin of this difference is not completely understood, we note that explicitly controlling the magnitude of the dilatational effects, made possible by the forcing examined here, may allow studies of compressibility effects relevant to both situations.

Since compressible turbulence simulations are much more expensive than incompressible simulations due to time step restrictions, the question of how to obtain the largest Reynolds number for a given grid size is even more pressing. To address this, full spectrum forcing was compared to its low-k restriction. In general, the conclusions are similar to those obtained in the incompressible case.[1] Thus, at a given resolution, low-k forcing produces much larger Reynolds numbers (almost double in the simulations presented here), so that one can more readily probe high Reynolds number asymptotics. In addition, for the compressible case, full spectrum linear forcing still requires Fourier transforms or Poisson solvers to split the velocity into solenoidal and dilatational components, so that its computational advantage is lost for real-space numerical codes. Nevertheless, low-k forcing components can be calculated without using a full Fourier transform, making it computationally more efficient.

The forcing presented here has been tested over a wide range of turbulent Mach numbers ($M_t = 0.02 - 0.6$), dissipation ratios ($\epsilon_d / \epsilon_s = 0.005 - 10$), and Reynolds numbers ($R_\lambda = 60 - 300$) with similar results. The method is stable, quickly adjusts to stationarity, and produces physical statistics that compare well with previous studies for the nearly incompressible cases. The effects of compressibility on the spectral dynamics and high order turbulence statistics will be discussed in a future paper.

ACKNOWLEDGMENTS

APPENDIX: FOURIER ANALYSIS OF ERRORS

The choice of resolution used for the simulations presented is based on a Fourier analysis of errors for compact finite difference schemes relative to spectral methods.[40,47] A one-dimensional periodic domain on $[0, L]$ is discretized by
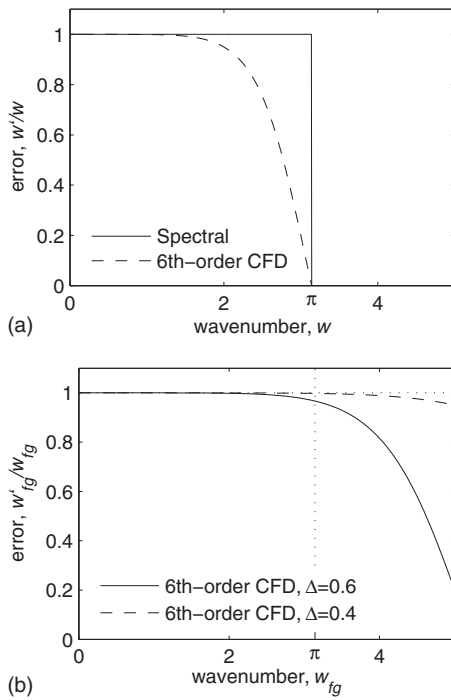
FIG. 12. Error in the modified wavenumber when the sixth-order compact finite difference scheme is on the same grid as a spectral method (a) and on a finer grid (b) with grid spacing contracted by a factor of Δ.

N grid cells of length $h=L/N$. For the sixth-order compact scheme used in this work, the derivative is computed using the approximation

$$\alpha f'_{l-1} + f'_l + \alpha f'_{l+1} = \frac{a}{2h}(f_{l+1}-f_{l-1}) + \frac{b}{4h}(f_{l+2}-f_{l-2}),$$

(A1)

with $\alpha=1/3$, $a=14/9$, and $b=1/9$,[40] where primes are derivatives and subscripts are grid indices.

Fourier coefficients $\hat{f}_k$ are defined such that

$$f(x) = \sum_{k=-N/2}^{N/2} \hat{f}_k \exp\left(\frac{2\pi i k x}{L}\right).$$

(A2)

It is convenient to scale the wavenumber as $w=2\pi k h/L = 2\pi k/N$ and the coordinate as $s=x/h$, so that $w \in [-\pi,\pi]$, and Fourier modes are $\exp(iws)$. The exact first derivative, with respect to s, has Fourier coefficients $\hat{f}'_k = iw\hat{f}_k$. The approximate derivative given by a finite difference scheme can be put in the form $(\hat{f}'_k)_{fd} = iw'\hat{f}_k$, where w' is a modified wavenumber that is a function of w and varies with the order of the scheme. For the sixth-order scheme

$$w'(w) = \frac{a\sin(w)+(b/2)\sin(2w)}{1+2\alpha\cos(w)},$$

(A3)

while for spectral methods,

$$w'(w) = w, \quad k \in [-\pi,\pi].$$

(A4)

The ratio w'/w is a measure of the error; spectral methods compute the exact derivative up to the Nyquist frequency $(w=\pi)$, while the accuracy of finite difference schemes,

when computed on the same grid, falls off at high wavenumbers [Fig. 12(a)]. To improve the accuracy of a finite difference scheme relative to the spectral method, one may increase the resolution: discretize the domain of length $[0,L]$ by a finer grid, with grid cells of width $h_{fg}=h\Delta$ using $N_{fg}=N/\Delta$ cells, where the contraction factor $\Delta<1$. Then the new wavenumbers $w_{fg}=w/\Delta$, and modified wavenumbers $w'_{fg}=w'/\Delta$ have a domain of $[-\pi/\Delta, \pi/\Delta]$.

$$w'_{fg}(w_{fg};\Delta) = \frac{a\sin(w_{fg}\Delta)+(b/2)\sin(2w_{fg}\Delta)}{\Delta[1+2\alpha\cos(w_{fg}\Delta)]}.$$

(A5)

The grid resolution is chosen such that the error w'_{fg}/w_{fg} is within acceptable limits. In practice, a grid size is chosen first, based on computational constraints, and then the Kolmogorov scale η is chosen such that the dissipation scale is well-resolved. The resolution of the spectral methods is usually given in terms of ηk_{max}. For example, $\eta k_{max}=1.0$, 1.5 corresponds to $\eta/h=0.32$, 0.48, respectively. The simulations presented here used $\eta/h_{fg}=0.8$. When compared to a spectral method using $\eta k_{max}=1.0$ [(Fig. 12(b)] this produces an error at the Nyquist frequency of less that 0.2% $(w'_{fg}/w_{fg}=0.998$ at $w_{fg}=\pi$ when $\Delta=0.4)$. Compared to a spectral method with $\eta k_{max}=1.5$, the Nyquist frequency error is less that 3.5% $(w'_{fg}/w_{fg}=0.966$ at $w_{fg}=\pi$ when $\Delta=0.6)$.

[1] Y. Kaneda and T. Ishihara, "High-resolution direct numerical simulation of turbulence," J. Turbomach. **7**, 20 (2006).

[2] V. Eswaran and S. B. Pope, "An examination of forcing in direct numerical simulations of turbulence," Comput. Fluids **16**, 257 (1988).

[3] T. Gotoh, D. Fukayama, and T. Nakano, "Velocity field statistics in homogeneous steady turbulence obtained using a high-resolution direct numerical simulation," Phys. Fluids **14**, 1065 (2002).

[4] A. Vincent and M. Meneguzzi, "Spatial structure and statistical properties of homogeneous turbulence," J. Fluid Mech. **225**, 1 (1991).

[5] T. S. Lundgren, "Linearly forced isotropic turbulence," *Annual Research Briefs* (Center for Turbulence Research, Stanford, CA, 2003), p. 461.

[6] R. M. Kerr, "Higher-order derivative correlations and the alignment of small-scale structures in isotropic numerical turbulence," J. Fluid Mech. **153**, 31 (1985).

[7] N. P. Sullivan, S. Mahalingam, and R. M. Kerr, "Deterministic forcing of homogeneous, isotropic turbulence," Phys. Fluids **6**, 1612 (1994).

[8] M. R. Overholt and S. B. Pope, "A deterministic forcing scheme for direct numerical simulations of turbulence," Comput. Fluids **27**, 11 (1998).

[9] K. R. Sreenivasan, S. I. Vainshtein, R. Bhiladvala, I. San Gil, S. Chen, and N. Cao, "Asymmetry of velocity increments in fully developed turbulence and the scaling of low-order moments," Phys. Rev. Lett. **77**, 1488 (1996).

[10] J. Jiménez, A. A. Wray, P. G. Saffman, and R. S. Rogallo, "The structure of intense vorticity in isotropic turbulence," J. Fluid Mech. **255**, 65 (1993).

[11] L. Machiels, "Predictability of small-scale motion in isotropic fluid turbulence," Phys. Rev. Lett. **79**, 3411 (1997).

[12] R. Rubinstein, T. T. Clark, D. Livescu, and L.-S. Luo, "Time-dependent isotropic turbulence," J. Turbomach. **5**, 11 (2004).

[13] C. Rosales and C. Meneveau, "Linear forcing in numerical simulations of isotropic turbulence: Physical space implementations and convergence properties," Phys. Fluids **17**, 095106 (2005).

[14] T. S. Lundgren, "Kolmogorov turbulence by matched asymptotic expansions," Phys. Fluids **15**, 1074 (2003).

[15] N. Kevlahan and R. E. Pudritz, "Shock-generated vorticity in the interstellar medium and the origin of the stellar initial mass function," Astrophys. J. **702**, 39 (2009).

[16] B. K. Shivamoggi, "Spectral laws for the compressible isotropic turbulence," Phys. Lett. A **166**, 243 (1992).

[17] D. Livescu, F. A. Jaberi, and C. K. Madnia, "The effects of heat release on the energy exchange in reacting turbulent shear flow," J. Fluid Mech. **450**, 35 (2002).

[18] F. A. Jaberi and C. K. Madnia, "Effects of heat of reaction on homogeneous compressible turbulence," J. Sci. Comput. **13**, 201 (1998).

[19] C. Federrath, R. S. Klessen, and W. Schmidt, "The density probability distribution in compressible isothermal turbulence: Solenoidal versus compressive forcing," Astrophys. J. **688**, L79 (2008).

[20] W. Schmidt, C. Federrath, M. Hupp, S. Kern, and J. C. Niemeyer, "Numerical simulations of compressively driven interstellar turbulence. I. Isothermal gas," Astron. Astrophys. **494**, 127 (2009).

[21] R. Benzi, L. Biferale, R. T. Fisher, L. P. Kadanoff, D. Q. Lamb, and F. Toschi, "Intermittency and universality in fully developed inviscid and weakly compressible turbulent flows," Phys. Rev. Lett. **100**, 234503 (2008).

[22] S. Kida and S. A. Orszag, "Energy and spectral dynamics in forced compressible turbulence," J. Sci. Comput. **5**, 85 (1990).

[23] X. D. Cai, E. E. O'Brien, and F. Ladeinde, "Advection of mass fraction in forced, homogeneous, compressible turbulence," Phys. Fluids **10**, 2249 (1998).

[24] B. R. Pearson, T. A. Yousef, N. E. Haugen, A. Brandenburg, and P.-Å. Krogstad, "Delayed correlation between turbulent energy injection and dissipation," Phys. Rev. E **70**, 056301 (2004).

[25] D. Porter, A. Pouquet, and P. Woodward, "Measures of intermittency in driven supersonic flows," Phys. Rev. E **66**, 026301 (2002).

[26] A. G. Kritsuk, M. L. Norman, P. Padoan, and R. Wagner, "The statistics of supersonic isothermal turbulence," Astrophys. J. **665**, 416 (2007).

[27] G. A. Blaisdell, "Numerical simulation of compressible homogeneous turbulence," Ph.D. thesis, Stanford Univ., CA, 1991.

[28] D. Livescu and C. K. Madnia, "Small scale structure of homogeneous turbulent shear flow," Phys. Fluids **16**, 2864 (2004).

[29] C. Cambon, G. N. Coleman, and N. N. Mansour, "Rapid distortion analysis and direct simulation of compressible homogeneous turbulence at finite Mach number," J. Fluid Mech. **257**, 641 (1993).

[30] C. Pantano and S. Sarkar, "A study of compressibility effects in the high-speed turbulent shear layer using direct simulation," J. Fluid Mech. **451**, 329 (2002).

[31] A. Simone, G. N. Coleman, and C. Cambon, "The effect of compresibility on turbulent shear flow," J. Fluid Mech. **330**, 307 (1997).

[32] S. Sarkar, "The pressure-dilatation correlation in compressible flows," Phys. Fluids **4**, 2674 (1992).

[33] P. G. Huang, G. N. Coleman, and P. Bradshaw, "Compressible turbulent channel flows: DNS results and modelling," J. Fluid Mech. **305**, 185 (1995).

[34] A. W. Vreman, N. D. Sandham, and K. H. Luo, "Compressible mixing layer growth rate and turbulence characteristics," J. Fluid Mech. **320**, 235 (1996).

[35] N. Masmoudi, "Asymptotic problems and compressible-incompressible limit," in *Advances in Mathematical Fluid Mechanics*, edited by J. Malek, J. Necas, and M. Rokyta (Springer, Berlin, 2000), pp. 119–158.

[36] D. Livescu, "Compressibility effects on the Rayleigh–Taylor instability growth between immiscible fluids," Phys. Fluids **16**, 118 (2004).

[37] H. Yu and D. Livescu, "Rayleigh–Taylor instability in cylindrical geometry with compressible fluids," Phys. Fluids **20**, 104103 (2008).

[38] G. Erlebacher, M. Y. Hussaini, H. O. Kreiss, and S. Sarkar, "The analysis and simulation of compressible turbulence," Theor. Comput. Fluid Dyn. **2**, 73 (1990).

[39] D. Livescu, Y. Khang, J. Mohd-Yusof, M. R. Petersen, and J. Grove, "CFDNS: A computer code for direct numerical simulation of turbulent flows," Los Alamos National Laboratory Technical Report No. LA-CC-09-100, 2009.

[40] S. K. Lele, "Compact finite difference schemes with spectral-like resolution," J. Comput. Phys. **103**, 16 (1992).

[41] J. R. Ristorcelli and G. A. Blaisdell, "Consistent initial conditions for the DNS of compressible turbulence," Phys. Fluids **9**, 4 (1997).

[42] R. Samtaney, D. I. Pullin, and B. Kosović, "Direct numerical simulation of decaying compressible turbulence and shocklet statistics," Phys. Fluids **13**, 1415 (2001).

[43] G. A. Blaisdell, N. N. Mansour, and W. C. Reynolds, "Compressibility effects on the growth and structure of homogeneous turbulent shear flow," J. Fluid Mech. **256**, 443 (1993).

[44] S. Sarkar, G. Erlebacher, M. Y. Hussaini, and H. O. Kreiss, "The analysis and modelling of dilatational terms in compressible turbulence," J. Fluid Mech. **227**, 473 (1991).

[45] Y. Kaneda, J. Yoshino, and T. Ishihara, "Examination of Kolmogorov's 4/5 law by high-resolution direct numerical simulation data of turbulence," J. Phys. Soc. Jpn. **77**, 064401 (2008).

[46] M. A. Taylor, S. Kurien, and G. L. Eyink, "Recovering isotropic statistics in turbulence simulations: The Kolmogorov 4/5th law," Phys. Rev. E **68**, 026310 (2003).

[47] A. W. Cook and P. E. Dimotakis, "Transition stages of Rayleigh–Taylor instability between miscible fluids," J. Fluid Mech. **443**, 69 (2001).